Two of the Five Zinc Fingers in the Zap1 Transcription Factor DNA Binding Domain Dominate Site-Specific DNA Binding†

M. V. Evans-Galea,‡,§ E. Blankman,‡,§ D. G. Myszka,|| A. J. Bird,^ D. J. Eide,*,^ and D. R. Winge*,§

Departments of Medicine and Biochemistry and Center for Biomolecular Interaction Analysis, University of Utah Health Sciences Center, Salt Lake City, Utah 84132, and Department of Nutritional Sciences, University of Missouri-Columbia, Columbia, Missouri 65211

Received June 18, 2002; Revised Manuscript Received September 19, 2002

ABSTRACT: The Zap1 transcriptional activator from *Saccharomyces cerevisiae* induces expression of a series of genes containing an 11 base pair conserved promoter element (ZRE) under conditions of zinc deficiency. This work shows that Zap1 uses four of its seven zinc finger domains to contact the ZRE and that two of these dominate the interaction by contacting the essential ACC-GGT ends. Two Zn finger domains (ZF1 and ZF2) do not contact DNA, and a third ZF3 may be more important for interfinger protein−protein interactions. Zn finger domains important for ZRE contact were identified from triple mutations in Zap1, changing three residues in the α helix in each finger known to be important for DNA contacts in Zn finger proteins. Replacement of −1, 3, and 6 helix residues in ZF4 and ZF7 reduced the affinity of Zap1 for the wild-type ZRE. In contrast, triple mutations within the intervening ZF5 and ZF6 domains had minimal effect. The data argue that fingers 4 and 7 contact the ACC-GGT ends while fingers 5 and 6 contact the 5 bp central ZRE sequence. This conclusion is corroborated by decreased Zap1 affinity for a ZRE DNA duplex containing mutations of the AC-GT ends of the ZRE, whereas transversion mutations within the central 5 bp of the ZRE had minimal effect on Zap1 binding affinity.

Zinc is an essential nutrient and is important for many different cellular functions. Zn(II) is an essential cofactor for zinc metalloenzymes and has a structural role in numerous proteins. Zinc deficiency is known in humans and results in adverse effects on growth and development (*1*). In contrast, accumulation of excess zinc can lead to toxic cellular effects. Thus, homeostatic mechanisms exist in cells to regulate the cellular concentration of zinc ions by maintaining zinc balance and minimizing deleterious effects of excess Zn(II) ions. Significant progress has been made recently to define the homeostatic mechanism for Zn(II) ions in the yeast *Saccharomyces cerevisiae*.

Regulation of Zn(II) homeostasis occurs, in part, at the level of Zn(II) uptake across the yeast plasma membrane. Two plasma membrane proteins, Zrt1 and Zrt2, are functional Zn(II) transporters (*2*, *3*). Zrt1 is required for high-affinity Zn(II) uptake, while Zrt2 encodes a low-affinity Zn(II) permease. Cellular Zn(II) levels regulate the expression of both *ZRT1* and *ZRT2* in addition to regulating protein levels of Zrt1 (*2*, *4*, *5*). Under Zn-deficient growth conditions, *ZRT1* and *ZRT2* are highly expressed, whereas their expression is inhibited in Zn-replete cells.

Sensing of zinc status is achieved through Zap1 in *S. cerevisiae* (*6*). Zap1 is a 93 kDa transcriptional factor that activates the expression of *ZRT1* and *ZRT2* in addition to over 40 other genes in Zn-deficient cells (*7*). The transcriptional activity of Zap1 is inhibited in Zn-replete cells. Cells lacking Zap1 are Zn-deprived due to attenuated expression of *ZRT1* and *ZRT2 (6)*. Zap1 binds in a sequence-specific manner to an 11 base pair element designated the zinc-responsive element (ZRE) (*5*). Zap1 target genes contain one or more copies of the ZRE consensus sequence 5′-ACCTTNAAGGT-3′ (*7*).

Five contiguous Cys_2His_2 zinc finger motifs found within a 194 amino acid segment near the C-terminus of Zap1 mediate high-affinity binding to a ZRE-containing DNA duplex (*8*). The importance of the C-terminal Zn finger domains for Zap1 function was highlighted by loss-of-function mutations substituting the two histidyl Zn ligands with glutamines in any one of these five Zn finger domains (*8*). In contrast, double His → Gln finger mutations in two additional Zn finger domains upstream and noncontiguous with the C-terminal five finger domains failed to attenuate ZRE/*lacZ* expression or DNA binding. Addition of a heterologous transactivation domain to the minimal five-finger DNA-binding domain of Zap1 activates *ZRT1* expression and confers Zn responsiveness when the fusion protein is not overexpressed (*9*). Thus, a Zn-responsive domain overlaps with the minimal five Zn finger DNA-binding domain.

† This work was supported by National Institutes of Health Grant R01 GM56285.

* To whom correspondence should be addressed. D.R.W.: Departments of Medicine and Biochemistry, University of Utah Health Sciences Center, Salt Lake City, Utah 84132; phone 801-585-5103; e-mail dennis.winge@hsc.utah.edu. D.J.E.: Department of Nutritional Sciences, 217 Gwynn Hall, University of Missouri−Columbia, Columbia, MO 65211; phone 573-882-9686; e-mail eided@missouri.edu.

‡ Contributed equally to the work.

§ Departments of Medicine and Biochemistry, University of Utah Health Sciences Center

|| Center for Biomolecular Interaction Analysis, University of Utah Health Sciences Center.

^ Department of Nutritional Sciences, University of Missouri.

10.1021/bi0263199 CCC: $25.00
Published on Web 01/07/2003

Although the five C-terminal Zn finger domains appear critical for *in vivo* function, it is unlikely that each finger is equally important in contacting the 11 base pair ZRE. Each zinc finger domain can potentially contact 3−4 base pairs (*10*−*14*). Three Zn finger motifs in Zif268 recognize successive base pair quartets covering a total of 10 bp (*10*, *12*). In Zif268 and selected Zif268 variants, the 4 bp site overlaps with the binding site of the neighboring Zn finger by one base pair (*15*). Three Zn finger domains of TFIIIA contact 11 bp (*16*). Thus, only a subset of the five Zn finger domains in the minimal DNA binding segment of Zap1 is likely responsible for base contact within the ZRE.

Not all multi-Zn finger domain proteins use Zn finger motifs equivalently in DNA binding. The Cys_2His_2 Zn finger motifs 4−6 in TFIIIA are positioned along the minor groove, rather than making major-groove base contacts (*16*). Likewise, the first of the five Cys_2His_2 Zn finger domains in the Gli transcriptional activator lies outside of the DNA major groove and makes no DNA contacts (*17*). The remaining four Zn fingers fit into the major groove, but two of those fingers make most of the base contacts of the 9-bp binding site (*17*). The Gli family (Gli1, Gli2, and Gli3) encodes zinc finger transcription activators that function as mediators of Hedgehog signaling in tissue patterning and stem cell specification in vertebrate embryos (*18*, *19*).

A combination of Zn finger−DNA structures and DNA site design/selection studies suggest that four residues in Cys_2His_2 Zn finger motifs are significant determinants in DNA base specificity (*10*−*14*). These four residues occupy positions −1, 2, 3, and 6 of the Zn finger α helix. The base contacts are either direct hydrogen bonds or water-mediated contacts (*12*). Additional residues make backbone contacts. In multi-Zn finger proteins, each finger uses a different combination of the four major contact residues to make most major-groove base contacts (*20*). The particular combination of contact residues in one finger making base contacts is dependent on the DNA base triplet sequence (*20*).

The novelty of Zap1 is that, in addition to using Zn finger motifs to contact DNA, the Zn finger domain is responsible for Zn regulation of transcription. The goal of the present study was to map the Zn finger domains in Zap1 responsible for ZRE base recognition to ultimately elucidate the Zn responsiveness of this protein.

MATERIALS AND METHODS

Growth Conditions and Vectors. Δ (MAT α *ade6 can1 his3 leu2 trp1 ura3 zap1*::*TRP1*) and the isogenic wild-type DY1457 were used (*6*). Yeast were grown in standard culture medium supplemented with 2% glucose and the appropriate auxotrophic requirements. Low-Zn medium was achieved in one of two ways. First, BIO101 medium lacking metal ions was used with all metal ions but Zn(II) replaced. Cells were cultured in this low-zinc medium with either 3 or 30 μM $ZnCl_2$ added. Second, EDTA was added to complete medium (CM) to a final concentration of 1 mM in addition to 10 μM $ZnCl_2$. Cells were cultured in this medium for 4 h prior to harvest. Stage of growth was determined by optical density of the liquid culture at 600 nm and converted to cell number by use of a standard curve. The Zap1 truncates (residues 538−880 and 687−880) and −1,3,6 mutant proteins were expressed in pGEX4T-1 (Pharmacia) via *Eco*RI and *Sal*I sites to generate N-terminal glutathione S-transferase (GST) fusions for protein purification. Expression of *ZAP1* and mutant variants in yeast was achieved by use of the centromeric YCp *URA3* vectors pRS416 containing the *ADH1* promoter and *CYC1* terminator (*21*) or a modified pRS316M25 vector containing the *MET25* promoter and *CYC1* terminator (*22*). Transformants with the pRS316M25 vector were cultured in methionine-containing medium to keep expression low.

Oligonucleotides. 5′-Biotinylated ZRE-containing oligonucleotides were chemically synthesized and complementary strands were annealed. The 31 bp ZRE duplex was the sequence of the ZRE1 of *ZRT1* (CCAAAGAT<u>ACCCTCAAGGT</u>TCTCATCTGTG) (*5*). The 11 bp ZRE is underlined. Two ZRE duplexes were synthesized with the 5′-biotinylated base at either end such that the duplex could be immobilized to streptavidin at either end. One of each pair of complimentary oligonucleotides was biotinylated via a TTATTA linker at the 5′ end for use in the Biacore studies. Four ZRE sequence variants were synthesized. The M2 mutant duplex contained the sequence CAAAGACCTTG inserted in place of the ZRE in the 31 bp duplex. The MM ZRE variant (MM for middle mutant) retained the palindromic end triplets but varied the central 5 bp of the ZRE, giving the sequence <u>ACC</u>TGAC<u>GGT</u>. The wild-type portions of the ZRE are underlined. The EM ZRE variant (EM, end mutant) altered the two terminal bases at each end of the ZRE, giving the sequence CT<u>CCTCAAG</u>AC. Two additional ZRE variants were synthesized as M2/ZRE hybrids in which each half of the ZRE was separately replaced with M2 sequences, thereby generating half-ZRE duplexes (ZRE/M2, <u>ACCCTC</u>GCTTG; M2/ZRE, CAAAG<u>CAAGGT</u>).

The QuikChange site-directed mutagenesis kit (Stratagene) was used with the specified oligonucleotides to generate the desired mutants. The pGEX4T-1 vector containing an N-terminal glutathione S-transferase (GST) fusion of *ZAP1* (codons 538−880) was used as the template for mutagenesis and subsequent expression in *Escherichia coli*. The *Bam*HI/*Hin*dIII fragments of the −1,3,6 Zn finger mutants were then subcloned into the same sites of the pRS416 vector (*21*). All constructs were sequenced for verification.

Zap1 Purification. When expressed in *E. coli*, the majority of each GST−Zap1 protein was found to be soluble. GST fusions were expressed in BL21(DE3) cells grown at 37 °C to an OD_{600} of 0.4 in the presence of 0.5 mM $ZnSO_4$ in LB medium. Following transfer to 30 °C, expression was induced with 0.4 mM IPTG and incubated for 3 h. Cells were harvested by centrifugation and washed in 0.25 M sucrose. The pellet was resuspended in buffer [20 mM NaH_2PO_4, 3.6 mM KH_2PO_4, pH 7.3, 280 mM NaCl, 5.4 mM KCl, 10% glycerol, and 5 mM dithiothreitol (DTT)] containing lysozyme and sonicated. The lysate was clarified by ultracentrifugation (100000*g*, 30 min, 4 °C) and purified on glutathione−Sepharose (Clontech). Eluted protein was concentrated in Viva-spin concentrators (MW cutoff 6000−8000), dialyzed against sonication buffer to remove GSH, and analyzed by SDS−12% PAGE. The protein was estimated to be >85% pure, and typically 6 L of cells would yield approximately 4 mg of protein. Where specified, the GST−$Zap1_{538-880}$ fusion was re-bound to GSH−Sepharose and incubated with thrombin (0.1 unit/μg of protein in sonication buffer) for 6

h at room temperature. Zap1 was of the expected molecular weight following cleavage of the N-terminal GST and was >95% pure. Zap1 proteins were stored in 5 mM DTT.

Sedimentation Equilibrium Ultracentrifugation. Purified Zap1 truncates were dialyzed against 2× phosphate-buffered saline (PBS) in the absence of DTT and glycerol. Ultracentrifugation was done at 28 000 rpm at 4°C in a Beckman Optima XL-A analytical ultracentrifuge with an AnTi60 rotor at 20 °C, in either 6-channel (12 mm thick) or double-sector (3 mm thick), charcoal-epon centerpieces. Sample channels contained multiple loading concentrations of Zap1 in PBS, while reference channels contained the dialysate. Loading concentrations varied between 4 and 16 μM in order to produce absorbance scans within the linear range of the detector at 280 nm. Samples were centrifuged until chemical equilibrium was attained. Cells were scanned radially in continuous mode, with data resulting from 10 absorbance readings taken at 0.001 cm intervals. Equilibrium was confirmed by no change in scans taken at 4 h intervals. Various models describing the concentration distribution were fit to final absorbance versus radius data by nonlinear least-squares techniques and the analysis program NONLIN (*23*). The final fit resulted from the simultaneous fitting of up to three different concentration distributions. To avoid the problem of relative local minima in the variance space, the fitting procedure was begun at many different initial points spanning the range of the parameters. The partial specific volume, 0.723 cm^3/g, was calculated from the amino acid sequence by the method described (*24*).

Electrophoretic Mobility Shift Assay. The standard 15 μL EMSA reaction contained hybridization mix [65 mM KCl, 0.2 mg/mL bovine serum albumin (BSA), and 20 mM Tris-HCl, pH 7.3, with 20% glycerol and 0.04% Igepal CA630 detergent] with end-labeled oligonucleotides and protein in sonication buffer. Following incubation at room temperature for 15 min, the samples were applied to a 6% polyacrylamide nondenaturing gel and electrophoresed for 1.5 h at 30 mA. Gels and running buffer contained 1× Tris−borate buffer, pH 8, and they were pre-electrophoresed for 1 h at 30 mA. A reaction lacking protein was used as a free probe (FP) control. Dried gels were viewed by autoradiography. To obtain the binding affinity, a series of 15 μL reactions were prepared containing different concentrations of protein in hybridization mix and radiolabeled oligonucleotides maintained at a constant DNA concentration. Reactions were allowed to reach equilibrium by incubation at room temperature for 15 min. The protein−DNA complex was then separated from free DNA by EMSA. Phosphorimages of dried gels were obtained and quantified with Quantity One software. The percentage of complex formation (as determined by the loss of free probe DNA) was plotted against concentration on a logarithmic scale to determine the apparent K_D.

Biacore Surface Plasmon Resonance Studies. A biomolecular interaction analyzing system instrument (Biacore 2000) was used to perform all binding studies. The biotinylated ZRE and scrambled duplex DNA were immobilized at various densities (15−875 RU) onto a streptavidin-containing CM5 sensor chip. Biacore equilibrium experiments were performed under the same buffer conditions as the electrophoretic mobility shift assays given above. Wild-type Zap1 and the variants were injected in the flow cells at concentrations from 1.5 μM to 0.36 nM depending on the construct. Each injection was repeated two or three times, with a 2 M NaCl regeneration between the binding cycles. The association data from the high-capacity surface was linear and highly flow-rate-dependent, indicating the reactions were limited by mass transport. Subsequent kinetic experiments were conducted with the low-capacity DNA surface (15 RU) and at a flow rate of 100 μL/min. All binding responses were processed with data from a reference surface as well as subtracting blank injections (*25*). Binding data were then fit globally, including a term for mass transport (*26*).

Zap1 Antibodies and Western. Adult New Zealand white rabbits were immunized by subcutaneous injection of 300 μg of purified $Zap1_{538-880}$ protein emulsified with an equal volume of Freund's complete adjuvant (Rockland). Immediately prior to injection, 0.5 mL of preimmune serum was collected. Six weeks after immunization, two booster injections of 0.5 mg of Zap1 mixed with incomplete adjuvant were given subcutaneously at 4-week intervals. The presence and specificity of the antibody were determined by Western analysis of WT and *zap1*Δ yeast extracts with antiserum obtained after the first booster injection. Ten days following the second booster, the animal was exsanguinated and polyclonal antisera were obtained. For Western analysis, yeast cells were cultured in either low-Zn medium (CM medium lacking uracil containing 1 mM EDTA and 10 μM $ZnCl_2$) or low-Zn medium supplemented with $ZnCl_2$. A concentration of the harvested cells, corresponding to 10^7 cells for transformants expressing Zap1 mutants in pRS316 or 4×10^6 cells for transformants expressing Zap1 mutants in pRS416, were denatured in SDS sample buffer in the presence of a protease inhibitor cocktail and 1.5 mM DTT. The samples were boiled for 5 min prior to loading on an SDS−12% polyacrylamide gel for electrophoresis. Proteins in the electrophoresed gel were blotted onto a nitrocellulose membrane followed by blocking in 3% milk/PBS/0.1% Tween for 1 h at room temperature. The blots were probed with a 1:1500 dilution of primary Zap1 antibody for 1 h at room temperature, followed by extensive washing with PBS and 0.1% Tween. The secondary antibody was an anti-rabbit antibody conjugated with horseradish peroxidase and this was added to the blot at a 1:3000 dilution in 3% milk/PBS/0.1% Tween. After being washed with PBS and 0.05% Tween, the blot was visualized with Pierce's SuperSignal West Dura extended duration substrate chemiluminescent reagents.

S1 Analysis. Total RNA was isolated from midlogarithmic cells by the hot acid phenol method and hybridized with ^{32}P-labeled, single-stranded *ZRT1* and *CMD1* (calmodulin) DNA oligonucleotides. *CMD1* was used as a loading control. The S1 probes used included 64 and 40 nucleotides of 5′ open reading frame (ORF) sequences of *ZRT1* and *CMD1*, respectively. This mixture was digested with the S1 nuclease and electrophoresed through an 8% polyacrylamide/5 M urea polyacrylamide gel. The data were visualized by autoradiography and quantified with a Bio-Rad FX Imager using Quantity One software. Ratios of *ZRT1* to *CMD1* expression levels were determined to quantify *ZRT1* transcript levels. The expression of *CMD1* is not modulated by the Zn status of cells.

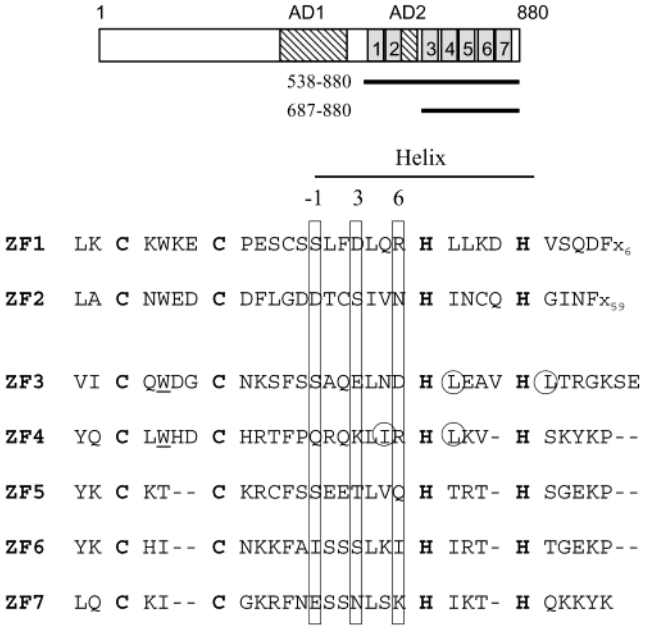

FIGURE 1: Scheme of Zap1 primary structure and the two protein constructs used in these studies (A, top panel). The two transactivation domains are hatched; the Zn finger motifs are boxed and numbered successively. (B, bottom panel) Sequences of the seven zinc finger motifs are shown; the Cys and His Zn(II) ligands are in boldface type. The position of the helix is shown by the bar, and the helical residues (positions −1, 3, and 6) mutated are boxed. The Trp residues predicted to make contacts in the β hairpin loops of ZF3 and ZF4 are underlined. The hydrophobic residues predicted to make interhelical hydrophobic contacts analogous to corresponding residues in Gli are circled.

RESULTS

A Functional Zap1 Truncate Binds the ZRE as a Monomer. An N-terminal truncate of Zap1 consisting of residues 538−880 is fully functional in vivo and confers Zn-dependent regulation on Zn regulon genes *(8)*. This truncate contains seven Zn finger motifs. The five most C-terminal Zn finger motifs form the minimal DNA binding domain (DBD) (Figure 1). DNA binding assays with the electrophoretic mobility shift assay (EMSA) previously revealed an apparent K_D in the 1−3 nM concentration range for Zap1 binding to a ZRE-containing DNA duplex (*8*). No difference in DNA binding was observed between Zap1 truncates containing only the five C-terminal Zn finger motifs and a longer construct containing all seven Cys_2His_2 Zn finger motifs (residues 538−880) (*8*).

The ZRE (5′-ACCTTNAAGGT-3′) has palindromic ends, so the initial question we addressed is whether Zap1 interacted with this palindromic sequence as an extended monomer or as a dimer with only a subset of Zn finger motifs in each monomer contacting each half of the ZRE. To test whether Zap1 binds to the ZRE as a monomer or dimer, two Zap1 truncates were expressed in *E. coli* and purified as GST fusion proteins. The truncates consisted of Zap1 residues 538−880 (ZF1−ZF7) and 687−880 (ZF3−ZF7). Following cleavage of the GST purification tag, the Zap1 polypeptides were isolated. DNA binding studies with the two length variants revealed a significant difference in the gel mobility of the protein−DNA complex (data not shown). The two truncates were mixed in varying ratios and tested by EMSA. The prediction was that if Zap1 binding to the ZRE occurred as a dimer, then a unique complex of intermediate mobility would exist with the mixture of two Zap1-length variants. However, mixtures of the two truncates varying in ratios failed to yield an intermediate complex, suggesting that either Zap1 binds to the ZRE as a monomer or each truncate was purified as a stable dimer (data not shown).

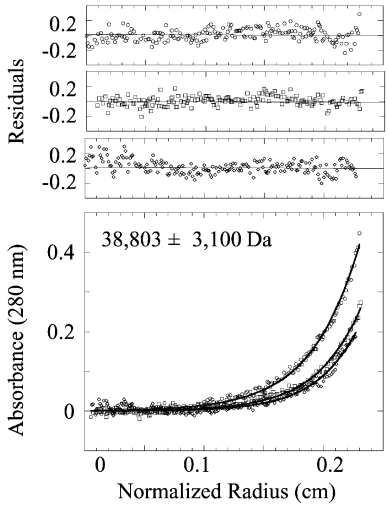

FIGURE 2: Analytical ultracentrifugation of $Zap1_{538-880}$. Three concentrations of Zap1 were used in the sedimentation equilibrium centriguation studies (4, 8, and 16 μM). The data were processed as described under Materials and Methods. The upper three panels show the residuals for the three samples from highest to lowest concentrations going from top to bottom (○, □, and ◇, respectively).

To discern between these two models, sedimentation equilibrium analysis was conducted with the Zap1 truncate (538−880) at three different protein levels. The protein was centrifuged until sedimentation and chemical equilibrium were attained. The best fit of the Zap1 data over the concentration range examined was obtained and indicated a monomeric species of molecular mass of 38 803 ± 3100 Da (Figure 2). The predicted mass of the Zap1 truncate is 39 445. The monomer fit gave small and randomly distributed residuals about zero. Thus, the functional $Zap1_{538-880}$ truncate exists in solution and binds the ZRE as a monomer.

Zap1/ZRE DNA Interactions Monitored by Surface Plasmon Resonance Analysis. The interaction of the two truncates with a ZRE DNA duplex was studied more thoroughly by surface plasmon resonance in a biomolecular interaction analyzing system. A 31 bp DNA duplex containing a central 11 bp ZRE was tethered to immobilized streptavidin on a gold surface biosensor chip through a terminal biotinylated base. The analyte was Zap1 delivered in a continuous flow over the sensor surface. Kinetic binding responses were recorded as the Zap1 protein associated with the immobilized DNA surface (Figure 3). The association phase was confined to the initial 30 s of analyte injection. After 30 s, the flow solution was changed to a buffer solution to monitor the dissociation of Zap1 from the ZRE surface. In Figure 3A, the binding curves shown are from 0 to 130 nM $Zap1_{538-880}$ with the ZRE duplex. Each concentration was injected twice to demonstrate the reproducibility of the assay. The surface capacity was intentionally kept very low to minimize mass transport effects. The random noise associated with low capacity surfaces has minimal effects on the reaction

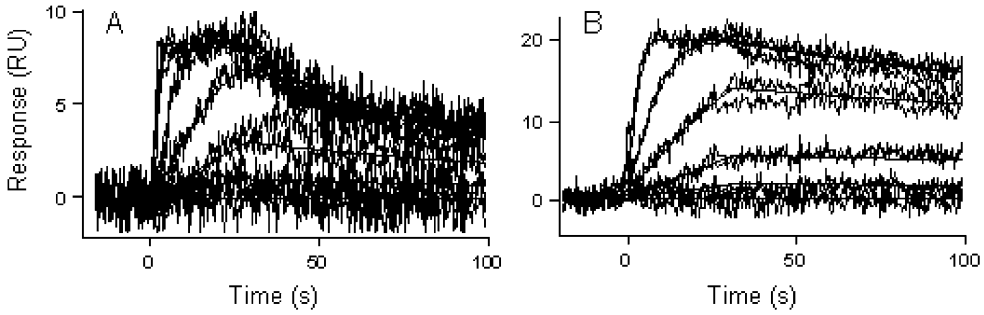

FIGURE 3: Interaction of Zap1 truncates with an immobilized ZRE DNA duplex by Biacore analysis. In panel A, the binding response for $Zap1_{538-880}$ at concentrations of 130, 43, 14.4, 4.8, and 0 nM injected in duplicate over a low-capacity ZRE DNA surface is shown. In panel B, the binding responses for $Zap1_{687-880}$ at concentrations of 215, 72, 24, 8, 2.65, and 0 nM injected in duplicate over ZRE DNA surface is shown. Quantitation of the data is shown in Table 1.

Table 1. Binding Constants for Zap1/DNA Interactions[a]

protein	DNA	figure	k_a (M^{-1} s^{-1})	k_d (s^{-1})	K_D (nM)
538−880	ZRE	3A	$5.7(0.2) \times 10^7$	$3.0(0.1) \times 10^{-2}$	0.5(0.3)
687−880	ZRE	3B	$3.8(0.1) \times 10^6$	$4.1(0.1) \times 10^{-3}$	1.09(0.04)
538−880	ZRE*	4A	$6.9(0.1) \times 10^7$	$1.40(0.02) \times 10^{-2}$	0.20(0.1)
538−880	MM	4B	$4.4(0.1) \times 10^6$	$4.91(0.01) \times 10^{-2}$	11.1(0.4)
ZF3	ZRE		$2.3(0.2) \times 10^7$	0.0084(0.0003)	0.36
ZF4	ZRE	7A	$1.9(0.1) \times 10^5$	$1.81(0.06) \times 10^{-1}$	967(60)
ZF4	MM	7A	nd	nd	nd
ZF5	ZRE	7B	$2.51(0.04) \times 10^7$	$1.66(0.02) \times 10^{-2}$	0.6(0.1)
ZF5	MM	7B	$2.69(0.08) \times 10^6$	$5.9(0.01) \times 10^{-2}$	22(1)
ZF6	ZRE	7C	$3.36(0.03) \times 10^6$	$4.54(0.04) \times 10^{-3}$	1.3(0.2)
ZF6	MM	7C	$1.01(0.03) \times 10^6$	$2.09(0.03) \times 10^{-2}$	20.6(0.8)
ZF7	ZRE	7D	$1.26(0.03) \times 10^7$	$2.1(0.05) \times 10^{-1}$	16.7(0.5)
ZF7	MM	7D	nd	nd	nd

[a] Zap1 truncates and mutant variants were tested for interaction with two DNA duplexes, either the wild-type ZRE duplex or the MM mutant duplex containing the wild-type palindromic end triplets but varied in the central 5 bp of the ZRE. The ZRE* indicates the experiment in which the wild-type ZRE duplex was biotinylated at the opposite end for immobilization on the streptavidin sensor chip. The actual data are derived from figures specified. The interaction of the ZF3 mutant is not shown. The numbers in parentheses indicate standard errors. nd, no detectable binding.

parameters (*27*). To extract binding kinetics, the experimental data were fit to a model of a 1:1 protein−DNA complex including a term for mass transport (Table 1) (*26*). The approximate dissociation constant (K_D) derived from the ratio of K_{off}/K_{on} was 0.5 ± 0.3 nM for $Zap1_{538-880}$. A second biotinylated ZRE duplex was generated with the biotinylated base at the opposite end of the duplex to address whether the immobilization of the ZRE duplex altered Zap1 binding affinity. Injection of $Zap1_{538-880}$ across the surface of this ZRE duplex surface resulted in a protein binding profile best fit with an apparent K_D of 0.2 ± 0.1 nM (Figure 4A). The similar affinity of Zap1 binding to the two duplexes immobilized at opposite ends indicates that immobilization did not markedly influence the binding process. No binding was detected for the Zap1 injected over a sensor surface bearing a mutant ZRE (M2) in which all 11 positions were altered by transversion mutations (data not shown). These data demonstrate that Zap1 binding to the wild-type ZRE was sequence-specific.

The interaction of the $Zap1_{687-880}$ truncate with the ZRE surface is shown in Figure 3B. The best fit of the data suggests an apparent K_D of 1.09 ± 0.04 nM. The similar binding constants of the two Zap1 truncates confirm that the two noncontiguous finger domains ZF1 and ZF2 do not influence DNA binding.

Binding studies were also carried out with ZRE sequence variants. The first variant (MM, middle mutant) retained the palindromic end triplets but varied the central 5 bp (ACC **CTCAA** GGT converted to ACC **TGACC** GGT; residues in boldface type were changed). The second variant (EM, end mutant) altered the two terminal bases at each end of the ZRE. Injection of Zap1 across the surface of the MM-ZRE duplex resulted in DNA binding curves that fit to K_D values of 11.1 nM (Figure 4B, Table 1). The binding isotherm for the interaction of $Zap1_{538-880}$ and the MM-ZRE duplex evaluated by EMSA yielded an apparent K_D of 16 nM (data not shown). In contrast, only low-affinity binding (>100 nM K_D) was observed for the EM mutant ZRE (data not shown). This mutant altered the ZRE sequence from **AC**C CTCAA G**GT** to **CT**C CTCAA G**AC**. The minimal Zap1 binding to the EM mutant ZRE, yet high affinity for the MM mutant ZRE with wild-type palindromic ends, highlights the importance of the AC ends of the ZRE element. Binding of Zap1 to DNA duplexes containing only half a ZRE was investigated. The DNA binding affinity of Zap1 binding to either ACC CTC**CC TTG** or **CAA AG**CAA GGT (bases in boldface type were changed) duplexes was reduced to 10 nM relative to the palindromic ZRE duplex (data not shown).

ZRE Binding by Zap1 Mutants with −1,3,6 Helix Substitutions. Only a subset of the five Cys_2His_2 Zn finger motifs in the minimal DBD is expected to make base-specific contacts with the 11 bp ZRE, since each finger can recognize 3−4 bp of DNA (*10*−*14*). Four residues of the Zn finger α helix, occupying positions −1, 2, 3, and 6, are major determinants in DNA base specificity (*10*−*15*). Different combinations of these contact residues make most major-groove base contacts (*15*, *20*). To map which Cys_2His_2 Zn finger motifs in Zap1 were responsible for specific base contacts within the ZRE, mutant Zap1 molecules were engineered with triple alanine substitutions at the −1, 3, and 6 positions of the finger helix (Figure 1B). Zap1 mutants were generated with triple Ala substitutions in each of the five DBD Zn finger motifs. The prediction was that a triple mutation within a single Zn finger would attenuate DNA binding if that particular Zn finger made significant base contacts. If a particular Zn finger did not make DNA contacts, such as Zn finger 1 of the Gli transcriptional factor, the prediction was that a triple mutation would not compromise DNA binding affinity. These mutations are not expected to alter the tertiary structure (see Discussion).

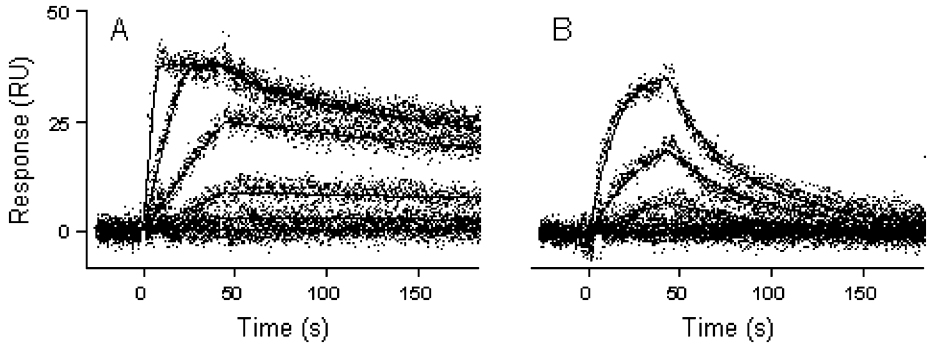

FIGURE 4: ZRE interaction of $Zap1_{538-880}$ with a ZRE DNA surface (panel A) and the MM mutant ZRE DNA surface (panel B) is shown. The ZRE duplex was biotinylated at the opposite end from the ZRE duplex used in Figure 4. Zap1 was injected at concentrations of 30, 10, 3.33, 1.11, 0.36, and 0 nM in triplicate over the two surfaces.

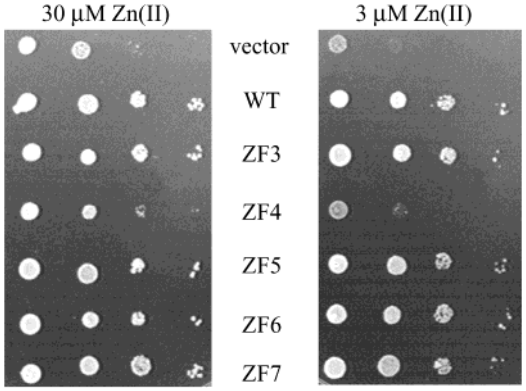

FIGURE 5: Complementation of *zap1*Δ cells by *ZAP1* mutants with −1,3,6 codon substitutions. Transformants were plated on low-zinc medium containing either 3 or 30 μM Zn(II). ZF3−ZF7 refers to −1,3,6 triple alanine substitutions in the particular Zn finger motif. The *ZAP1* mutants were expressed from a YCp vector controlled by the *ADH1* promoter and terminator.

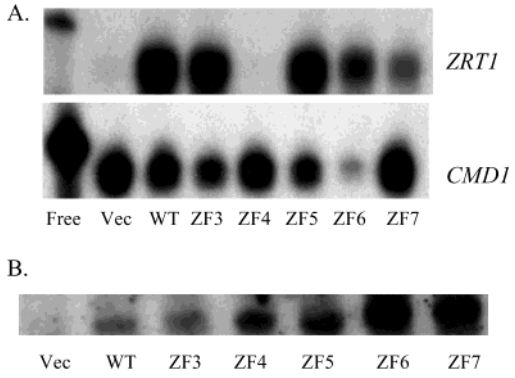

FIGURE 6: (A) S1 nuclease assay of *ZRT1* expression in *zap1*Δ cell transformants containing *ZAP1* mutants with −1,3,6 codon substitutions. Transformants were cultured in CM medium and incubated with 1 mM EDTA and 10 μM $ZnCl_2$ for 4 h prior to harvest. *CMD1* was used as a loading control. *ZRT1* expression was quantified relative to *CMD1* transcript levels that do not change in a Zn-dependent manner. (B) Lysates from the transformants were probed by Western analysis to quantify Zap1 protein levels. Equal quantities of total protein were loaded in each lane. This was confirmed by doing immunoblotting with Pgk1 (data not shown).

Triple Zap1 mutants were evaluated for function by in vivo studies and in vitro DNA binding studies. The triple mutants of *ZAP1* (codons 538−880) were expressed from a YCp vector under the control of the *ADH1* promoter and terminator. Expression of the triple mutants in a *zap1*Δ strain revealed that only the ZF4 triple mutant failed to complement the *zap1*Δ cells for growth in low-Zn(II) medium (Figure 5). The transformants were also tested for *ZRT1* expression in cells cultured in low-Zn(II) medium. As expected, *ZRT1* expression monitored by the S1 nuclease protection assay was absent in *zap1*Δ cells containing an empty vector (Figure 6A). *ZRT1* expression was at wild-type levels in transformants containing ZF3, ZF5, and ZF6 triple mutants, suggesting that these mutant Zap1 proteins were functional for DNA binding in vivo. In contrast, *ZRT1* expression was absent in the ZF4 triple mutant and significantly reduced (5-fold) in the ZF7 triple mutant. The reduced *ZRT1* expression in the ZF4 and ZF7 triple mutants was not a result of reduced Zap1 protein levels (Figure 6B). In fact, the mutant proteins accumulated to somewhat higher levels than the wild-type Zap1 protein.

The in vivo results of the triple mutants are consistent with ZF4 and ZF7 being most important for ZRE recognition. To confirm this conclusion, the Zap1 triple mutants were purified after expression in *E. coli*. DNA binding studies with each triple-mutant protein was carried out by Biacore analysis. ZRE binding by ZF3 and ZF5 mutant Zap1 proteins was quantitatively similar to that of wild-type Zap1 with apparent K_D values below 1 nM (Table 1). The affinity of the ZF6 mutant for ZRE was slightly reduced, 1.3 nM (Table 1), yet this mutant was indistinguishable from the wild-type protein in the in vivo assays above. In contrast, the apparent K_D values of ZRE binding by the ZF4 and ZF7 triple mutants were 967 and 16.7 nM, respectively (Figure 7A,D and Table 1). Comparable results were obtained with the ZRE duplex immobilized at the opposite end (data not shown). Thus, triple mutations in ZF4 had the most deleterious effects in ZRE binding in vitro and *ZRT1* expression in vivo, with the triple mutations in ZF7 having a smaller but still significant inhibitory effect.

The triple-mutant proteins were also tested with the MM mutant ZRE duplex immobilized on the biosensor surface. The wild-type Zap1 bound the MM mutant ZRE with an apparent K_D of 11.1 ± 0.4 nM. Both ZF5 and ZF6 triple-mutant proteins bound the MM duplex with K_D values close to 20 nM (Table 1). Thus, ZF5 and ZF6 triple mutants mimicked wild-type Zap1 in ZRE binding in vitro and *ZRT1* expression in vivo. In contrast, no binding was observed for either ZF4 or ZF7 triple-mutant proteins with the MM duplex even at high protein concentrations.

Candidate Interfinger Interactions between ZF3 and ZF4 in Zap1. The results with the −1,3,6 triple mutants are consistent with Zn finger motifs 4 and 7 being dominant in

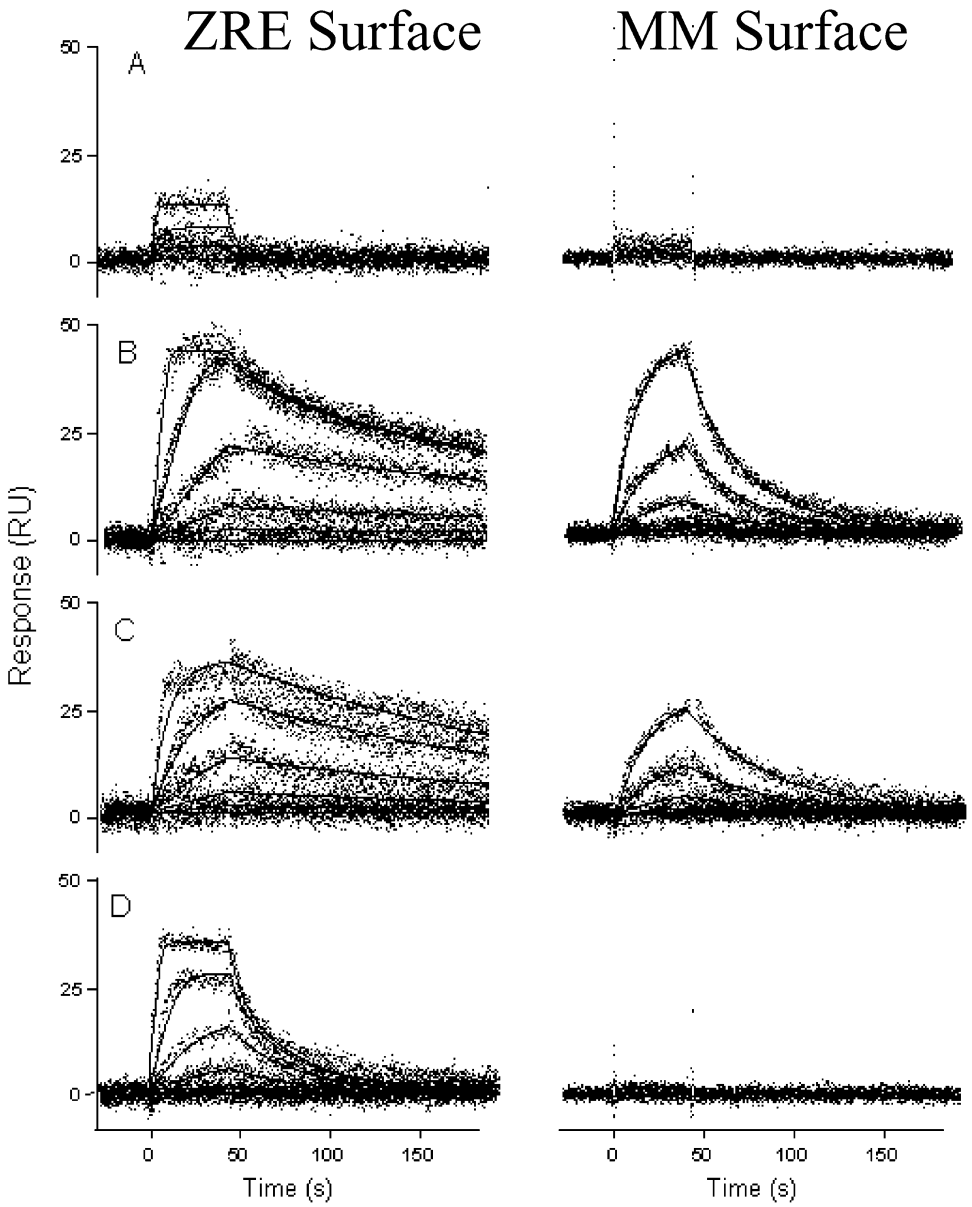

FIGURE 7: Mutant Zap1 protein/DNA interactions. The panels represent the following: (A) ZF4 Zap1 mutant (1.5, 0.5, 0.16, 0.055, 0.018, and 0 μM); (B) ZF5 Zap1 mutant (36, 12, 4, 1.33, 0.44, and 0 nM); (C) ZF6 Zap1 mutant (30, 10, 3.33, 1.11, 0.36, and 0 nM); and (D) ZF7 Zap1 mutant (118, 39, 13, 4.37, 1.46, and 0 nM). The left and right panels refer to protein injected over ZRE and MM DNA surfaces, respectively.

ZRE recognition and likely contacting one or more bases in the terminal ACC triplets. ZF3 is unlikely to be responsible for base contacts. ZF3 differs from ZF4−ZF7 in having a nine-residue spacer separating ZF3 and ZF4. A common theme in multi-Zn finger proteins is that Zn finger motifs responsible for base contacts within the major groove are linked to adjacent Zn finger domains by seven residues (*16*). A DNA backbone contact is frequently made by a conserved Lys residue within the linker (*12*); this conserved Lys is not present in the ZF3/ZF4 spacer. Not only is the linker elongated between ZF3 and ZF4 in Zap1, the sequence does not resemble that of a typical spacer separating two major-groove-binding Zn finger motifs.

The Zap1 ZF3 domain resembles more closely the first Zn finger of the Gli activator. ZF1 in Gli does not make DNA contacts; rather, it makes protein−protein contacts with the DNA-contacting ZF2 (*17*). The packing interface between Gli ZF1 and ZF2 consists of a contact between two Trp residues in the β-hairpin loops between the two cysteinyl residues in ZF1 and ZF2 and a hydrophobic interhelical packing between the two helices of ZF1 and ZF2 (*17*). The β-hairpin loops of Zap1 ZF3 and ZF4 contain Trp residues positioned similarly, and the helical residues contributing to the hydrophobic packing in Gli are likewise apolar residues in Zap1 (Figure 1B). One prediction is, therefore, that ZF3 and ZF4 in Zap1 pack together similarly to ZF1 and ZF2 in Gli. The hydrophobic interhelical packing of ZF1 and ZF2 in Gli leaves accessible a separate helical face containing the side chains of helical residues −1, 2, 3, and 6. Thus, mutations in the ZF3 −1,3,6 residues would not be expected to affect interhelical packing or DNA binding as we observed.

To test the significance of the predicted interface between Zap1 ZF3 and ZF4, the Trp residues and adjacent residues in the two β-hairpin loops (Trp^{709} and Trp^{742}) were altered (Figure 1B, Trp residues underlined). The β-hairpin loop in

ZF3 sequence QWDG was changed to QSKG to remove the Trp residue and adjacent Asp that may make a stabilizing salt bridge with the ZF4 β-hairpin loop. The β-hairpin loop in ZF4 was changed from LWHD to LSKN to remove the Trp and alter adjacent residues that may also be part of β-hairpin loop contact. The second set of mutations focused on the hydrophobic residues contributing to the predicted interhelical hydrophobic contacts between ZF3 and ZF4. Leu^{726} and Leu^{731} of ZF3 and Ile^{756} and Leu^{759} of ZF4 were mutated to aspartates (mutated residues shown in italic type in Figure 1B). Double mutations were engineered in minimal *ZAP1* (codons 538−880) and the mutant genes were subcloned in a yeast centromeric (YCp) vector under the control of the *MET25* promoter and terminator. Transformants of *zap1*Δ cells with *ZAP1* and mutant variants were tested for *ZRT1* expression and Zap1 protein stability. Neither the β-hairpin loop mutant proteins nor the interhelical packing mutants were stable, making functional studies impossible. The loss of β-hairpin loop and interhelical packing destabilized Zap1.

Two other unusual features of ZF3 in Zap1 are the four-residue spacing between the histidyl Zn(II) ligands and the long spacer between ZF3 and ZF4. The four-residue spacer between His residues in ZF3 is expected to distort the helix to permit His ligation to Zn(II) (*28*). Three of the Zn fingers in TFIIIA show this *i*, *i* + 5 spacing between the two helical His residues, and these helices show localized underwinding to accommodate this spacing (*16*). To determine whether these two unusual features of Zap1 Zn finger motifs was important for Zap1 function, we first constructed a Zap1 mutant to reduce the spacing between these two His residues to the traditional *i*, *i* + 4 His spacing by deletion of the Glu in the LEAV spacer. Second, to evaluate the interfinger spacing, the SE in the linker was deleted, converting the linker from LTRGKSEYQ to LTRGKYQ. Neither mutation had an effect on Zap1 function or Zap1 protein stability. The two mutant proteins were equally effective in activating *ZRT1* expression and suppressing the growth defects of *zap1*Δ cells on low-Zn medium (data not shown).

DISCUSSION

Our results not only substantiate previous findings that indicate the full DBD of Zap1 was Zn finger domains 3−7 but also show that Zap1 binds the ZRE as a monomer. Furthermore, we have determined the role each finger plays in specific recognition of the 11 base pair ZRE sequence. On the basis of the consensus sequence derived by Lyons et al. (*7*), we predicted that the most important bases in the sequence for site-specific Zap1 binding were the ACC-GGT ends. These sequences are the most conserved and we find them to be of greatest importance for site-specific DNA binding in vitro.

Given the size of the ZRE, we predicted that only a subset of fingers bind to DNA, and this was supported by our mutational analysis of Zap1. Four of the five Zn finger domains in the minimal DBD appear to contact the ZRE. Curiously, ZF3 does not appear to make major-groove DNA contacts. ZF3 resembles finger 1 of Gli, which makes interfinger protein−protein contact and no DNA contacts. Of fingers 4−7, we found that fingers 4 and, to a lesser extent, 7 play the major roles in contacting the ZRE.

Zf7	Zf6,5	Zf4	Zf3
6 -1		6 -1	
KNE		RKQ	
ACC	TTnAA	GGT	
TGG	AAnTT	CCA	

FIGURE 8: Scheme of how Zap1 Zn finger motifs 4−7 may interact with the 11 base pair ZRE.

Mutations in these fingers greatly reduced the affinity of Zap1 for the wild-type ZRE. Mutations in fingers 5 and 6 had little effect, suggesting that these fingers are far less important in site-specific binding. The data argue that fingers 4 and 7 contact the ACC-GGT ends while fingers 5 and 6 contact the 5 bp core sequence of the ZRE. This conclusion is supported by several observations. First, the linear way in which ZF proteins bind to DNA suggests that fingers 4 and 7 will contact the ends of the site. Second, mutations in ZF4 and ZF7 had major effects on DNA binding as did mutation of the AC-GT ends of the ZRE. Third, mutations in the central region had far lesser effects, as did mutation of ZF5 or ZF6. The MM ZRE mutation reduced the affinity of wild-type Zap1 by about 10-fold. A similar effect was observed on the binding of ZF5 and ZF6 mutants to the MM ZRE, suggesting that little additional perturbation of binding occurred when both the ZRE and the fingers were mutated. Likewise, sequence variation is seen in the middle 5 bp of natural ZREs and these sequence variations do not diminish the effectiveness of a ZRE (*5*). Fourth, whereas wild-type Zap1 bound the MM ZRE with only a modest drop in affinity, the ZF4 or ZF7 mutants failed to bind to the MM ZRE. Fifth, Zap1 binding to half-ZRE duplexes was reduced 10-fold, a similar drop in affinity as a mutant lacking ZF7 function. Since the ZRE is palindromic, we anticipate that ZF4 dominates the Zap1 interaction with half-ZRE duplexes. The summation of these results demonstrates clearly the dominance of ZF4 and ZF7 in ZRE recognition, with the intervening ZF5 and ZF6 domains making lesser contributions to ZRE interaction. The use of DNA binding helix mutations to map the important interface for ZRE interactions is not expected to alter the structure of the Zn fingers as this face of the helix projects away from the tertiary fold of the Zn fingers. Furthermore, replacing these residues with Ala in a minimalist Zn finger peptide did not alter the tertiary structure (*29*).

Additional indirect evidence is consistent with the conclusion that Zn finger domains ZF4−ZF7 contact the ZRE. First, the linkers between ZF4 and ZF5, ZF5 and ZF6, and ZF6 and ZF7 conform to the typical seven-residue spacing (residues separating second His of one finger from the first Cys of the adjacent finger) found in Zn fingers that contact major-groove DNA sites and contain the conserved basic residue important for backbone DNA contacts (*16*). The spacer between ZF3 and ZF4 is nonstandard (nine residues) and lacks the basic residue for backbone DNA contact. Second, recognition of ACC ends by ZF4 and ZF7 is consistent with base recognition rules established by site-selection studies (*30*, *31*). One model for the ZRE recognition is shown in Figure 8. If ZF4 contacts the terminal GGT in the 5′-ACCTTNAAGGT, the −1, 3, and 6 residues, Gln, Lys, and Arg, may be expected to contact the base triplet in an antiparallel fashion resulting in Gln−T and Arg−G contacts. These are reasonable hydrogen-bonding contacts

based on site selection studies (*30*, *31*). ZF7 may contact the opposite ACC triplet through Glu (−1), Asn (3), and Lys (6) helix residues. Hydrogen bonding by Glu and Asn with C bases is reasonable on the basis of published site-selection studies (*31*). Many site-selection studies are based on Zif268 variants in which DNA contacts are primarily on one strand. Other Zn finger proteins contact both strands (*14*), so one cannot be certain whether the Zn finger motifs in Zap1 will exhibit the Zif268 type of DNA contacts.

If DNA contact is restricted to ZF4−ZF7, an obvious question is what roles ZF3 and the upstream ZF1/ZF2 finger pair have. The ZF1/ZF2 finger pair is interdigitated within a transcriptional activation domain. Recent evidence suggests ZF1/ZF2 is involved in Zn regulation of the transcriptional activation function of Zap1.[1] ZF3 appears analogous to the first Zn finger motif in Gli. The Gli ZF1 does not contact DNA; rather, it forms a series of stabilizing interactions with ZF2 that does contact DNA (*17*). The ZF1/ZF2 interfinger contacts in Gli consist of contacts of two Trp residues (oriented in perpendicular fashion) in the β-hairpin loops of the two Zn finger motifs and interhelical packing with hydrophobic contacts (*17*). These contact residues in Gli are conserved in ZF3 and ZF4 in Zap1. The loss of Zap1 stability in mutant variants with substitutions in the putative contact residues is expected if ZF3/ZF4 in Zap1 were packed together as ZF1/ZF2 in Gli. ZF3 in Zap1 may function in anchoring ZF4 for DNA contacts. This may account for the greater observed contribution of ZF4 in ZRE recognition than ZF7. Interfinger interactions are known to organize the protein−DNA interaction (*15*). An interfinger contact in Zif268 is thought to orient an Arg residue for DNA contact (*15*).

An important unresolved question with Zap1 is the mechanism by which Zn(II) inhibits Zap1 DNA binding function. A number of scenarios arise from this present work. Disruption of the ZF3/ZF4 finger pair may abrogate DNA binding. Alternatively, the ZF3/ZF4 interfinger contact may create an interface for an inhibitory interaction with a regulatory protein. Gli interacts with a second molecule Zic1 that may be involved in transcriptional regulation, but this contact is outside the finger pair (*32*). Further studies are needed to resolve the mechanism of Zn regulation of Zap1 function.

ACKNOWLEDGMENT

We acknowledge Dr. David Stillman for many useful discussions and Dr. Lisa Joss for assistance in sedimentation equilibrium ultracentrifugation.

REFERENCES

1. Keen, C. L., and Gershwin, M. E. (1990) *Annu. Rev. Nutr. 10*, 415−431.
2. Zhao, H., and Eide, D. (1996) *J. Biol. Chem. 271*, 23203−23210.
3. Zhao, H., and Eide, D. (1996) *Proc. Natl. Acad. Sci. U.S.A. 93*, 2354−2458.
4. Gitan, R. S., Luo, H., Rodgers, J., Broderius, M., and Eide, D. (1998) *J. Biol. Chem. 273*, 28617−28624.
5. Zhao, H., Butler, E., Rodgers, J., Spizzo, T., Duesterhoeft, S., and Eide, D. (1998) *J. Biol. Chem. 273*, 28713−28720.
6. Zhao, H., and Eide, D. J. (1997) *Mol. Cell. Biol. 17*, 5044−5052.
7. Lyons, T. J., Gasch, A. P., Gaither, L. A., Botstein, D., Brown, P. O., and Eide, D. J. (2000) *Proc. Natl. Acad. Sci. U.S.A. 97*, 7957−7962.
8. Bird, A., Evans-Galea, M. V., Blankman, E., Zhao, H., Luo, H., Winge, D. R., and Eide, D. J. (2000) *J. Biol. Chem. 275*, 16160−16166.
9. Bird, A. J., Zhao, H., Luo, H., Jensen, L. T., Srinivasan, C., Evans-Galea, M., Winge, D. R., and Eide, D. J. (2000) *EMBO J. 19*, 3704−3713.
10. Pavletich, N. P., and Pabo, C. O. (1991) *Science 252*, 809−816.
11. Fairall, L., Schwabe, J. W., Chapman, L., Finch, J. T., and Rhodes, D. (1993) *Nature 366*, 483−487.
12. Elrod-Erickson, M., Rould, M. A., Nekludova, L., and Pabo, C. O. (1996) *Structure 4*, 1171−1180.
13. Elrod-Erickson, M., and Pabo, C. O. (1999) *J. Biol. Chem. 274*, 19281−19285.
14. Houbaviy, H. B., Usheva, A., Shenk, T., and Burley, S. K. (1996) *Proc. Natl. Acad. Sci. U.S.A. 93*, 13577−13582.
15. Wolfe, S. A., Grant, R. A., Elrod-Erickson, M., and Pabo, C. O. (2001) *Structure 9*, 717−723.
16. Nolte, R. T., Conlin, R. M., Harrison, S. C., and Brown, R. S. (1998) *Proc. Natl. Acad. Sci. U.S.A. 95*, 2938−2943.
17. Pavletich, N. P., and Pabo, C. O. (1993) *Science 261*, 1701−1710.
18. Kinzler, K. W., and Vogelstein, B. (1990) *Mol. Cell. Biol. 10*, 634−642.
19. Ruiz i Altaba, A., Palma, V., and Dahmane, N. (2002) *Nat. Rev. Neurosci. 3*, 24−33.
20. Elrod-Erickson, M., Benson, T. E., and Pabo, C. O. (1998) *Structure 6*, 451−464.
21. Ronicke, V., Graulich, W., Mumberg, D., Muller, R., and Funk, M. (1997) *Methods Enzymol 283*, 313−322.
22. Mumberg, D., Muller, R., and Funk, M. (1994) *Nucleic Acids Res. 22*, 5767−5768.
23. Johnson, M. L., Correia, J. J., Ypahantis, D. A., and Halvorson, H. R. (1981) *Biophys. J. 36*, 575−588.
24. Laue, T. M., Shah, B. D., Ridgeway, T. M., and Pelletier, S. L. (1992) *Computer aided interpretation of analytical sedimentation data for proteins*, Ultracentrifugation in Biochemistry and Polymer Science (Harding, S. E., Rowe, A. J., and Horton, J. C., Eds.) pp 90−125, Cambridge University Press, Cambridge, U.K.
25. Myszka, D. G. (1999) *J. Mol. Recognit. 12*, 279−284.
26. Myszka, D. G., He, X., Dembo, M., Morton, T. A., and Goldstein, B. (1998) *Biophys. J. 75*, 583−594.
27. Myszka, D. G., Jonsen, M. D., and Graves, B. J. (1998) *Anal. Biochem. 265*, 326−330.
28. Norregaard, L., Visiers, I., Loland, C. J., Ballesteros, J., Weinstein, H., and Gether, U. (2000) *Biochemistry 39*, 15836−15846.
29. Michael, S. F., Kilfoil, V. J, Schmidt, M. H., Amann, B. T., and Berg, J. M. (1992*) Proc. Natl. Acad. Sci. U.S.A. 89*, 4796−4800.
30. Choo, Y., and Klug, A. (1994) *Proc. Natl. Acad. Sci. U.S.A. 91*, 11168−11172.
31. Choo, Y., and Klug, A. (1994) *Proc. Natl. Acad. Sci. U.S.A. 91*, 11163−11167.
32. Koyabu, Y., Nakat, K., Mizugishi, K., Aruga, J., and Mikoshiba, K. (2001) *J. Biol. Chem. 276*, 6889−6892.

[1] A. Bird et al., manuscript in preparation.

BI0263199